coatings

Article

Effect of Glymo on the Morphological and Optical Properties of Eu^{3+}-Doped Lu_2SiO_5 Films

Andrea Danielle Cancino-Moreno [1,†], Arturo López-Marure [1,†], Jorge Humberto Luna-Domínguez [2], Ángel de Jesús Morales-Ramírez [3], Mayahuel Ortega-Avilés [4], José Alfredo Álvarez-Chávez [5] and Margarita García-Hernández [6,*]

1 Instituto Politécnico Nacional-CICATA Altamira, Carretera Tampico-Puerto Industrial Altamira, Altamira Tamaulipas 89600, Mexico
2 Facultad de Odontología, Universidad Autónoma de Tamaulipas, Centro Universitario Tampico-Madero, Av. Universidad Esq. Blvd. Adolfo López Mateos, S/N, Tampico, Tamaulipas 89337, Mexico
3 Instituto Politécnico Nacional, Escuela Superior de Ingeniería Química e Industrias Extractivas, Av. Luis Enrique Erro, S/N, UPALM, Ciudad de Mexico 07738, Mexico
4 Instituto Politécnico Nacional, Centro de Nanociencias y Micro y Nanotecnologías, Av. Luis Enrique Erro S/N, Nueva Industrial Vallejo, Gustavo A. Madero, Ciudad de Mexico 07738, Mexico
5 Optical Sciences Group—University of Twente, Drienerlolaan 5, 7522NB Enschede, The Netherlands
6 Instituto Politécnico Nacional, CECyT 16 "Hidalgo" Ciudad del Conocimiento y la Cultura, Carretera Pachuca Actopan Km 1+500, San Agustín Tlaxiaca Hidalgo 42162, Mexico
* Correspondence: margarciah@ipn.mx; Tel.: +00-52-55-57-29-60-00 (ext. 83808)
† These authors contributed equally to this work.

Abstract: Eu^{3+}-(5% mol)-doped Lu_2SiO_5 optical quality films were prepared using the sol–gel method and dip-coating technique from lutetium and europium salts as the lanthanide precursors and tetraethyl orthosilicate (TEOS) as the silicon source. To increase the thickness of the films, 3-Glycidyloxypropyl trimethoxysilane (Glymo) was added as the rheological agent during sol formation. Structural, morphological, and luminescent properties were investigated for Lu_2SiO_5, Eu^{3+}:Lu_2SiO_5, and Eu^{3+}:Lu_2SiO_5/Glymo in order to obtain high quality in luminescent films. X-ray diffraction (XRD) results show that the incorporation of the Eu^{3+} ions do not affect the A-Type and B-Type monoclinic crystalline phase typical of Lu_2SiO_5, even after five dipping cycles on quartz substrates and a final annealing process at 1100 °C. The morphology and topography of the films were studied by SEM and AFM. These techniques revealed films without surfactant that were uniform with low rugosity while the film with surfactant presented porous hills and valleys with uneven high values of roughness. The photoluminescence spectrum of Eu^{3+}:Lu_2SiO_5 films showed 2 broad emission peaks centered at 589 nm and 612 nm. The presence of Glymo in the system promoted the formation of residual $Lu_2Si_2O_7$ compounds with the highest lifetime values compared with films without surfactant. The results of the films are promising for luminescent applications.

Keywords: Lu_2SiO_5 films; sol–gel; Glymo; luminescence

check for updates

Citation: Cancino-Moreno, A.D.; López-Marure, A.; Luna-Domínguez, J.H.; Morales-Ramírez, Á.d.J.; Ortega-Avilés, M.; Álvarez-Chávez, J.A.; García-Hernández, M. Effect of Glymo on the Morphological and Optical Properties of Eu^{3+}-Doped Lu_2SiO_5 Films. *Coatings* **2023**, *13*, 915. https://doi.org/10.3390/coatings13050915

Academic Editor: Alicia de Andrés

Received: 21 April 2023
Revised: 4 May 2023
Accepted: 8 May 2023
Published: 12 May 2023

1. Introduction

In the last few decades, a large number of luminescent materials consisting of oxides [1] and doped with rare earth ions have been studied due to their exceptional properties and potential applications such as in fluorescent lamps, LEDs, emissive displays, and medical imaging as X-ray detectors. However, it is well stated that the most promising form for these materials is in thin films because the optical resolution is higher compared with particulate systems, showing higher contrast, as well as excellent adhesion to the substrate surface [2,3]. Rare earth silicate phosphors have stimulated the interest of researchers since the Lu_2SiO_5:Ce^{3+} phosphor discovery by Melcher and Schweitzer in 1992 [4] because of its great luminescent performance. Structurally, Lu_2SiO_5 consists of isolated SiO_4 tetrahedrons surrounded by Lu atoms which can be coordinated with six or seven oxygen atoms (Lu1 and Lu2 sites) conforming the typical monoclinic structure for this system [5]; this ceramic material has a high density of 7.4 g/cm^3, thermal stability, and high yield emission [6,7], with Lu_2SiO_5 being a promising material for this application. The high density and great ability to be doped with rare earth ions enable the production of new phosphor materials. What makes lutetium silicate an attractive host is that it presents similar characteristics to commercial phosphors, such as the fast response of BaF_2, the high light output of Gd_2O_2S:Tb, and the high density of $Bi_4Ge_3O_{12}$. Besides the chemical stability and transparency, which allows the Lu_2SiO_5 system to be doped with rare earth ions such as Eu^{3+}, researchers are searching for red emissions for possible application in optoelectronic devices [3,8–10]. Since the typical route of the synthesis of this phosphor is using a solid-state reaction, nevertheless, it is not adequate to produce transparent films. However, rare-earth ions-doped Lu_2SiO_5 phosphors have been synthesized by other methods, such as hydrothermal [11], pulsed laser deposition (PLD) [12], the Pechini sol–gel method [3], Czochralski [4], and the float-zone method [9].

The aim of this investigation is to study the microstructural properties of the sol–gel films as a function of the luminescent yield. For the first time, pure and doped Lu_2SiO_5 films were synthesized and modified with Glymo as a surfactant. The films were grown on quartz substrates and heat treated reaching a temperature of 1100 °C to ensure crystallization according to the phase diagram of rare earth silicates by Felsche [13]. The main reaction for the formation of the Lu–Si–Glymo complex is proposed for the first time. The structural characteristics were analyzed by X-ray diffraction. Scanning electron and atomic force microscopies (SEM and AFM) were employed to identify the morphology and topography of the obtained films. PL studies were recorded in order to observe the emission lines of europium ions when excited in the UV wavelength range.

2. Materials and Methods

2.1. Preparation of the Films

Lu_2SiO_5, $Lu_2SiO_5:Eu^{3+}$, and $Lu_2SiO_5:Eu^{3+}$/Glymo phosphor samples were prepared by the sol–gel method and the dip-coating technique. Lutetium oxide (Lu_2O_3), nitric acid (HNO_3, 99.9%), tetraethyl orthosilicate (TEOS $Si(OC_2H_5)_4$, 99%), europium nitrate ($Eu(NO_3)_3$, 99.9%), ethanol (C_2H_5OH, 99%), and acetylacetone (Acac $C_5H_8O_2$, 99%) were used as starting materials. Glycidyloxypropyl trimethoxysilane (Glymo) was used as a surfactant modifier of sol viscosity. The doping concentration of Eu^{3+} was 5% mol and the Glymo:Lu_2SiO_5 molar ratio was 1.3. The luminescent lutetium silicate films were prepared according to Figure 1.

The elaboration of Lu_2SiO_5 was carried out in two steps. Firstly, the Lu_2O_3 sol was prepared by dissolving Lu_2O_3 powder in concentrated HNO_3; the reaction took place under vigorous stirring and heating (100 °C) to obtain $Lu(NO_3)_3$ crystals [14]. Then, 0.5 mmol of $Lu(NO_3)_3$ was mixed in ethanol and AcAc as the chelating agent in a Lu:AcAc molar ratio of 1:1 under vigorous stirring for an hour [14–16]. In the second part, the SiO_2 sol was prepared from 2 dissolutions: (1) an amount of 7.6 mL of TEOS was added to ethanol (molar ratio TEOS:ethanol = 1:4) and (2) HCl was added to deionized water with a molar ratio of 530:1 of H_2O:HCl, respectively. Each dissolution was stirred for an hour, and then both dissolutions were mixed and stirred for 21 h [17]. Afterwards, 1 mol of Lu_2O_3 sol and 1 mol of SiO_2 sol were mixed and stirred for 2 h [18]. Finally, an appropriate amount of Eu^{3+} ions were introduced to the obtained *sols* and also the surfactant was added according to Table 1.

In Figure 2, the main reactions of lutetium silicate formation by mean of the sol–gel method are presented. In Figure 2A,B, the hydrolysis and condensation reaction of lutetium oxide and silicon oxide is shown. In Figure 2C, the reaction mechanism of lutetium silicate is proposed. As can be observed in Figure 2C, water and ethanol solvate the alkoxy group from TEOS being protonated and the electronic density of TEOS is favored towards the oxygen atoms; therefore, the silicon acquires an electrophilic character, thus becoming more susceptible to attack by solvents [19].

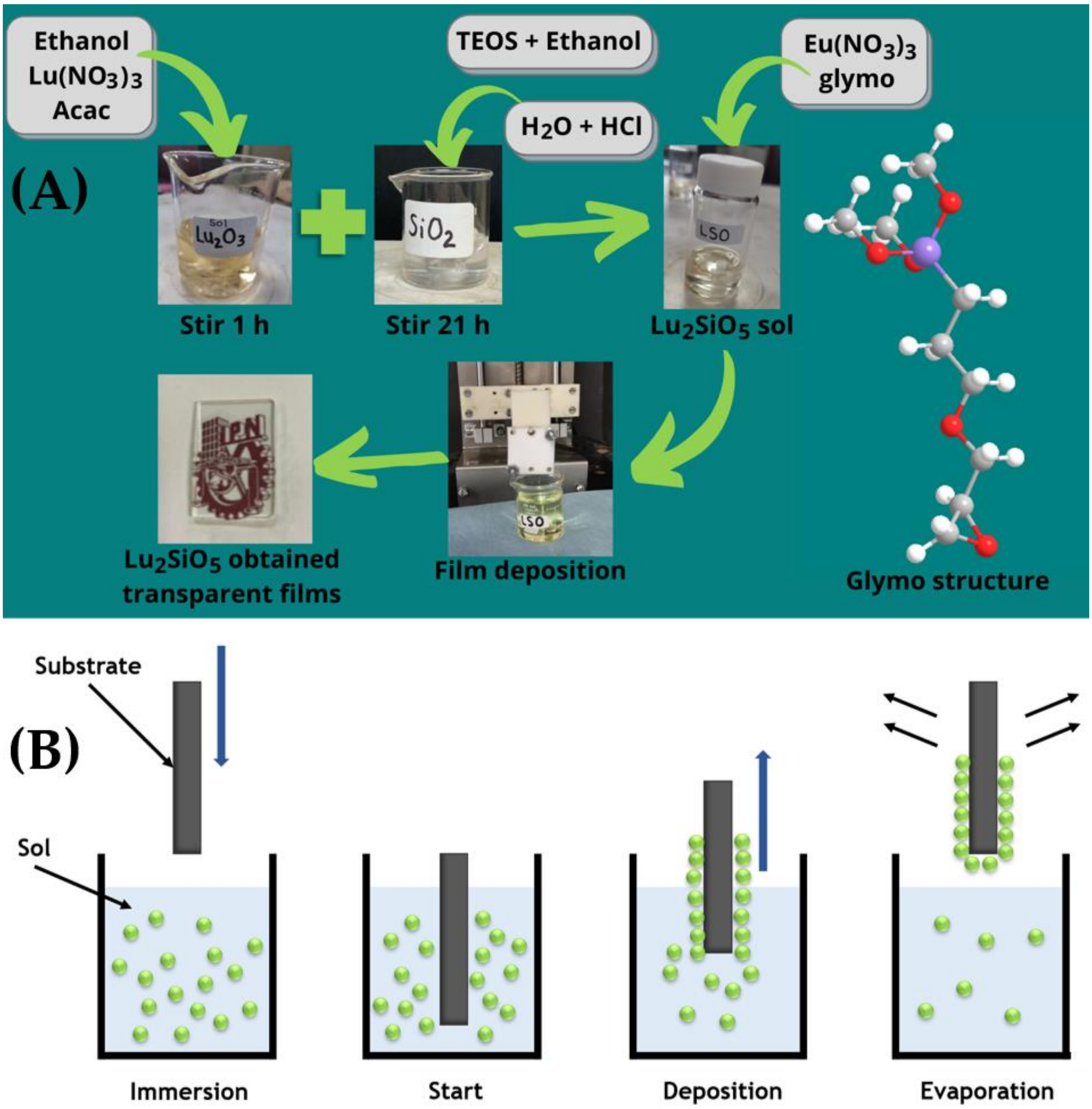

Figure 1. (**A**) Schematic representation of the procedure steps to elaborate Eu-doped Lu_2SiO_5 films by the sol–gel method and dip-coating technique and (**B**) scheme of the main steps for film deposition by the dip-coating technique.

Table 1. Name label and molar conditions used for the elaboration of Lu_2SiO_5 powder and films.

Type	Matrix	Sample	Eu^{3+} (%Mol)	Glymo:Lu_2SiO_5 (Molar Ratio)	# Dips
Film	Lu_2SiO_5	LS1	-	-	5
Film	Lu_2SiO_5	LS2	5	-	5
Film	Lu_2SiO_5	LSG2	5	1.3	5
Powder	Lu_2SiO_5	p-LS1	-	-	-
Powder	Lu_2SiO_5	p-LS2	5	-	-
Powder	Lu_2SiO_5	p-LSG2	5	1.3	-

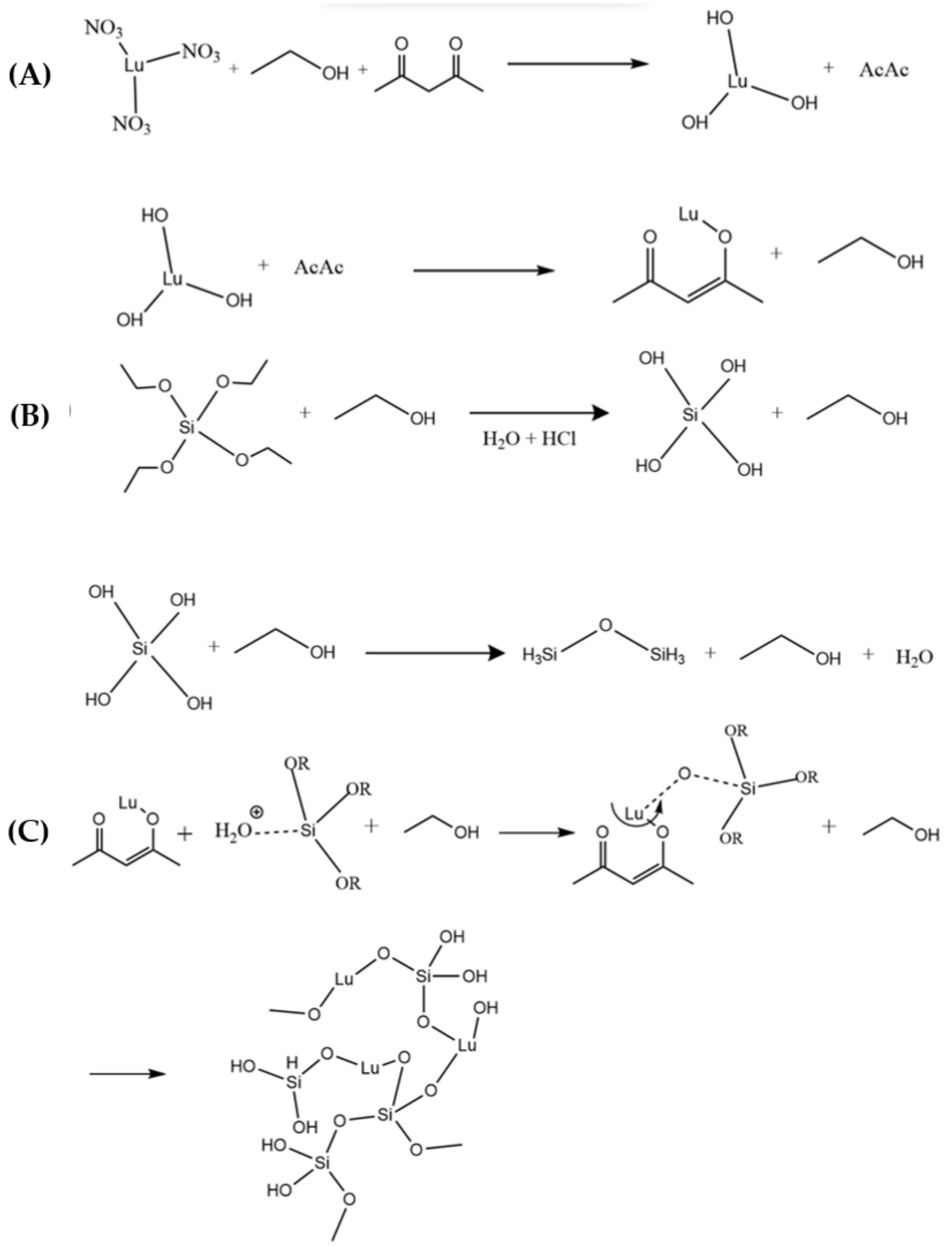

Figure 2. Schematic representations of the main reactions for (**A**) lutetium oxide, (**B**) silicon oxide, and (**C**) lutetium silicate formation through the sol–gel method.

When lutetium is in contact with silicon oxide sol, it can be attracted to oxygen from alkoxy groups displaced from the chelating agent, thus forming a new silicium–lutetium complex. This complex later becomes a precursor of the three-dimensional network of the solvated gel by the combination of water and ethanol in an aqueous medium. The obtained sol was filtered using a 0.2 mm syringe filter to elaborate the highly transparent and stable precursor solution ready for deposition on quartz glass substrates (QSI quartz, Quartz Scientific Inc., Lake Country, OH, USA). The substrates were cleaned using a special protocol prior deposition stage in order to obtain optical and reproducible films [20]. The substrates were dip coated following the steps according to Figure 1B and using a withdrawal speed of 0.5 cm s^{-1} for all films. After dipping the films were dried at 100 °C for 10 min to remove the most volatile solvents as water and alcohol; this procedure was repeated for each coating up to 5 cycles.

In the 5th and last coat, the films were annealed from 300 °C to 1100 °C for 10 min at each temperature at an interval of 200 °C obtaining a high-quality transparent film as shown in Figure 3. The films without Glymo (Figure 3A,B) revealed a homogenous and transparent surface, while the films containing Glymo as a surfactant showed a compromised film quality as can be observed in Figure 3C.

(A) (B) (C)

Figure 3. Images of the (**A**) synthesized Lu_2SiO_5, (**B**) Eu^{3+}:Lu_2SiO_5, and (**C**) Eu^{3+}:Lu_2SiO_5/Glymo films obtained after annealing to 1100 °C.

2.2. Preparation of Powders

After the film preparation, the remnant sol was dried at 100 °C for 24 h. The obtained xerogel were calcined at 300 °C, 500 °C, 700 °C, 900 °C, and 1100 °C for 2 h at each temperature in order to obtain the Lu_2SiO_5 crystalline powders labeled according to Table 1.

2.3. Characterization

The crystalline structure of the samples was characterized by X-ray diffraction (XRD) using a powder diffractometer Bruker D8 Advance with Cu k_α radiation (λ = 1.5418 Å) at a scan rate of 0.02° between 10 and 80° at 2q. The morphology of the crystalline films and the topography were measured using a Quanta FEG 250 Scanning Electron Microscope operated at 15 kV and an atomic force microscope Nanosurf Naio AFM equipment directly on the film's surface in a tapping mode. The photoluminescence studies were carried out with an F-7000 FL Spectrophotometer, Hitachi High-Technologies Corporation, Tokyo, Japan.

3. Results and Discussions

Figure 4 shows the XRD patterns for the p-LS1, p-LS2, and p-LSG2 powders calcined at 1100 °C. Two different phases of Lu_2SiO_5, A-type and B-type, were identified. A monoclinic phase was identified for the powder systems, and the presence of 2 different symmetries, P21/c and C2/c, was due to an incomplete phase transition from the A-type (P21/c) to the B-type (C2/c) Lu_2SiO_5 (Figure 4B). The addition of Glymo as a surfactant influenced the crystalline phase as shown on the XRD pattern of the pLSG2 sample, benefiting the formation of the A-type $Lu_2Si_2O_7$ (Figure 4C). This can be explained by the proposed reaction of the precursor solution and Glymo (Figure 5). Based on the characteristic peak of the Lu_2SiO_5 system at 2θ = 30.15°, the crystallite sizes of the p-LS1, p-LS2, and p-LSG2 samples were obtained according to Scherrer's formula [21]:

$$D = \frac{k * \lambda}{\beta * \cos\theta} \quad (1)$$

where D is the average crystallite size, k is the shape factor constant (typically equal to 0.9), λ is the X-ray wavelength, β is peak width at FWHM, and θ is the Bragg angle.

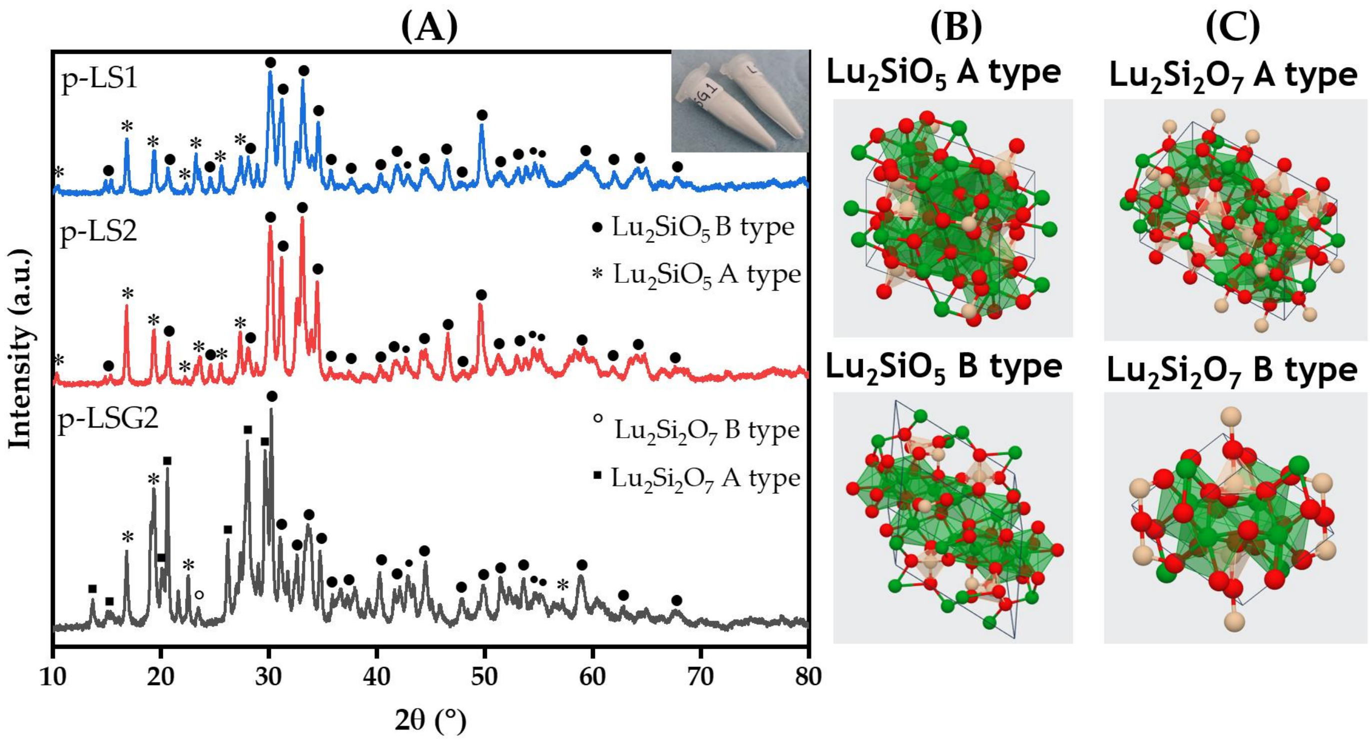

Figure 4. XRD patterns of the (**A**) Lu_2SiO_5 powder systems calcined at 1100 °C for 2 h, (**B**) Lu_2SiO_5 A and B types of monoclinic structures, and (**C**) $Lu_2Si_2O_7$ A type of tetragonal and B type of monoclinic structures.

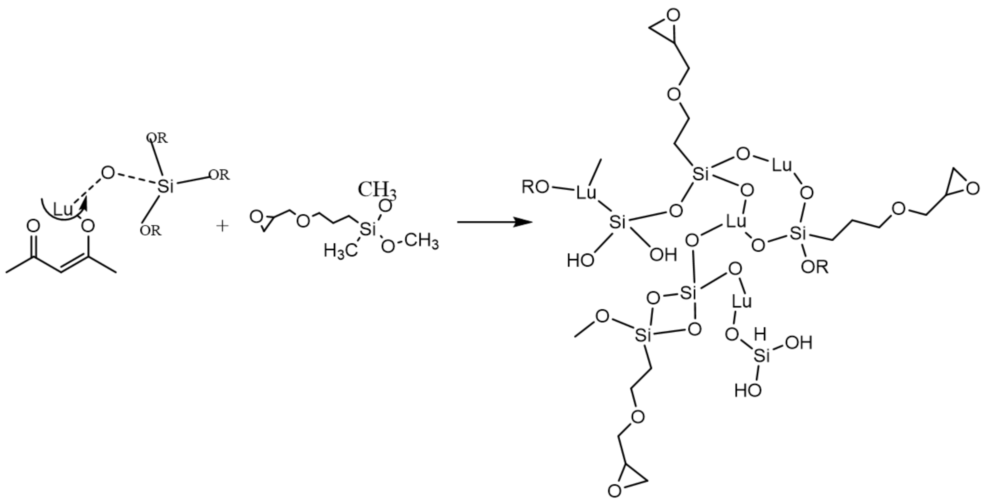

Figure 5. Scheme of the lutetium silicate reaction into the sol formation stage using Glymo.

The average crystallite sizes of the p-LS1, p-LS2, and p-LSG2 systems were 14 nm, 16 nm, and 36 nm, respectively. In addition to the crystalline phase, the incorporation of Glymo as a surfactant has an influence on the crystallite size, which increases in relation to the pure and doped system with Eu^{3+}. Due to the addition of Glymo as a surfactant, a Lu–Si–Glymo complex is formed, where Glymo acts as a crosslinker agent.

According to the reaction mechanism proposed for the formation of the precursor solution (Figure 5), the addition of Glymo favors the growth of the 3D network that will form the gel, obtaining a larger crystallite size compared with systems that do not contain Glymo. Figure 6A illustrates the X-ray diffraction patterns of pure, Eu-doped, and Eu-doped (Glymo) Lu_2SiO_5 films calcined at 1100 °C. The broad signal from ≈ 10–30° is ascribed to the amorphous structure of quartz substrates [22–24]. Characteristic peaks of the B-type Lu_2SiO_5 were identified according to the standard diffraction data (ICSD #279584) for the LS1 and LS2 samples.

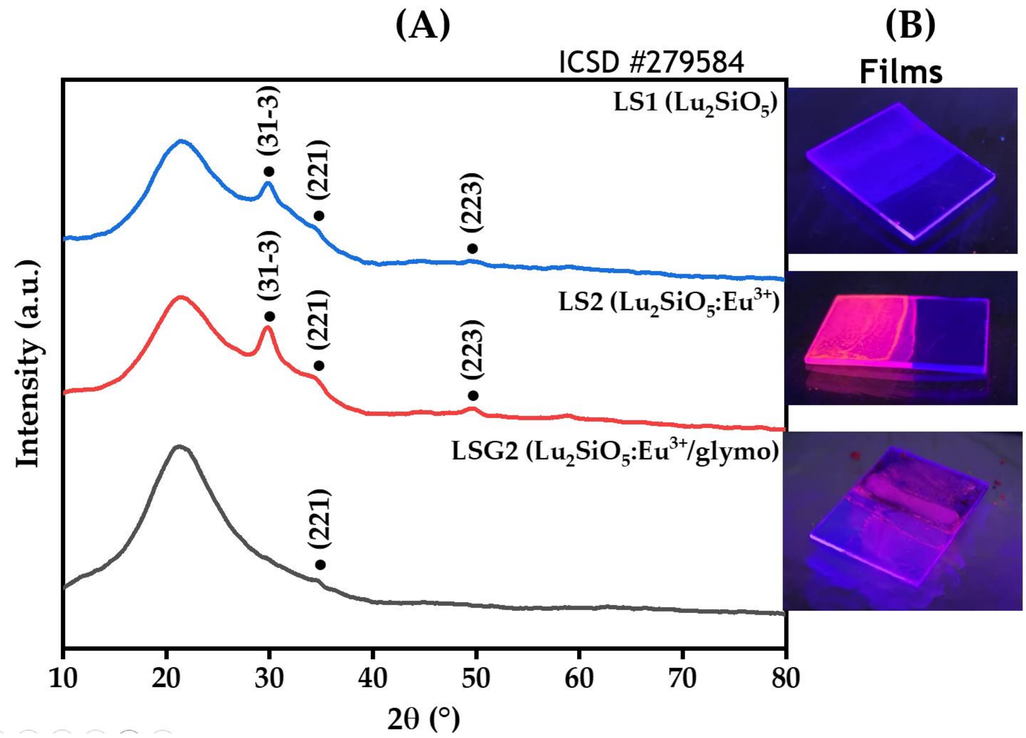

Figure 6. (**A**) XRD patterns and (**B**) luminescence images excited by UV lamp at 254 nm of the Lu_2SiO_5 films heat treated at 1100 °C for 10 min.

When the Glymo was incorporated into the system as a surfactant (LSG2 sample), a weak diffraction peak of the B-type Lu_2SiO_5 was identified at 2θ = 34.77°. This peak is related to the phase transition into the A-type $Lu_2Si_2O_7$, which is observed in Figure 4A when the same system is prepared as a powder. It is known that the typical and stable phase of Lu_2SiO_5 is the B-type (C2/c symmetry). For the LS1 and LS2 film systems, the typical phase is obtained, even with the incorporation of the Eu^{3+}. Europium ion does not affect the crystalline phase due to the similar atomic radius between the Lu atoms and the Eu^{3+} ions. A shift in the signals on the XRD pattern does not exist, which suggests that the Eu^{3+} ions successfully substituted the Lu atoms of the host.

It is important to note that the B-type monoclinic structure of the Lu_2SiO_5 film was obtained at 1100 °C by the sol–gel method, i.e., a lower calcined temperature compared with other preparation methods previously described such as the combustion method. Xu et al. obtained the Lu_2SiO_5 system at 1550 °C [25], spark plasma sintering at 1350 °C was obtained by Jianjun Xie et al. [26], a solid-state reaction at 1300 °C was synthesized by Yinzhen Wang et al. [27], and a pressure-less sintering was proposed by Lingcong Fan et al. with a thermal treatment at 1500 °C [28]. Furthermore, even by the sol–gel method, the common obtaining temperature for Lu_2SiO_5 is 1200 °C as previously reported by Xiaolin Liu et al., C. Mansuy et al., and Xiaoxing Zhang et al. [29–31].

Figure 7 reveals the surface morphology by SEM observations of monolayer $Lu_2SiO_5:Eu^{3+}$ (a), monolayer $Lu_2SiO_5:Eu^{3+}$/Glymo (b), and mapping of the $Lu_2SiO_5:Eu^{3+}$ film (c).

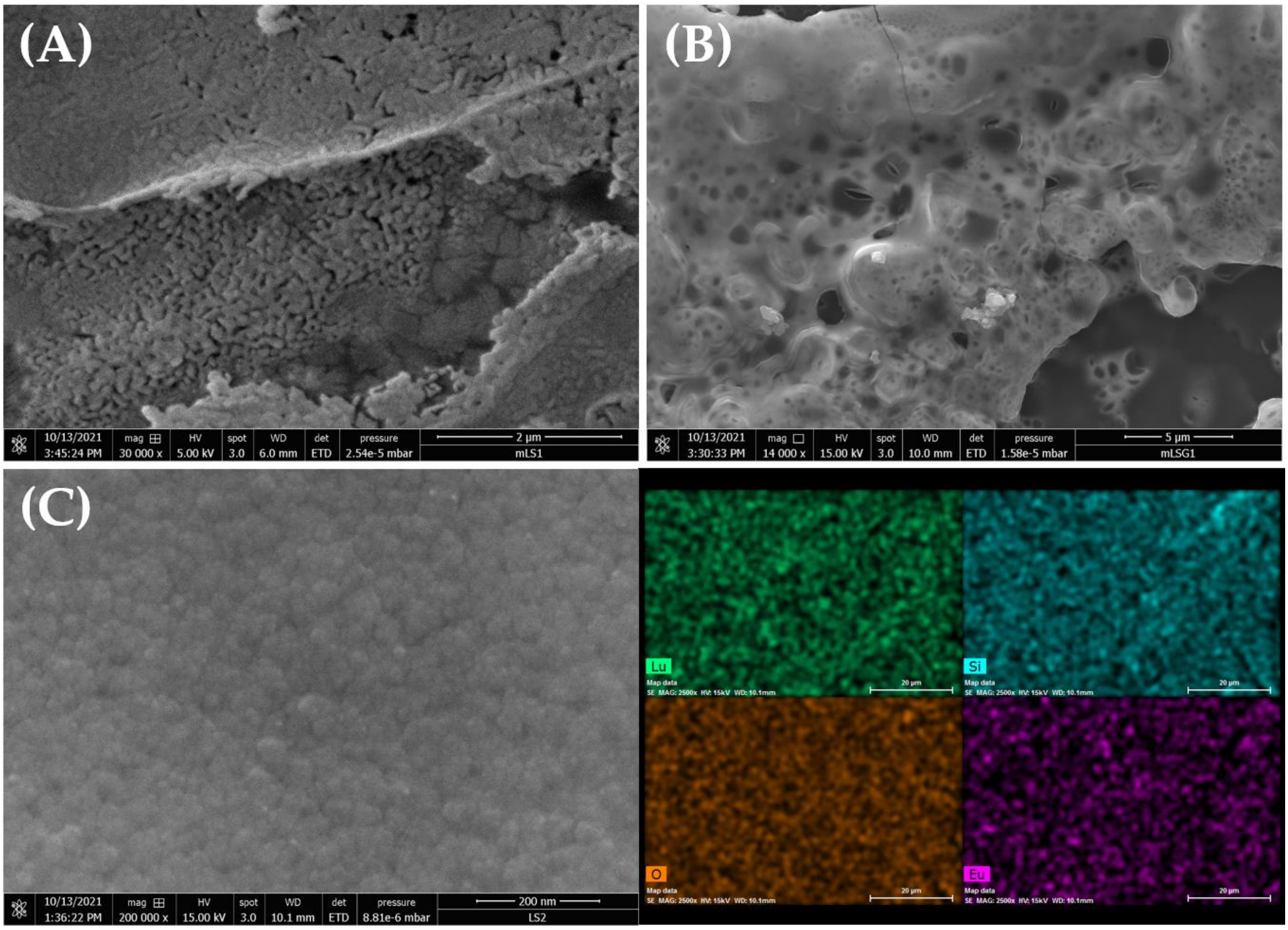

Figure 7. SEM images of (**A**) monolayer Eu^{3+}:Lu_2SiO_5, (**B**) monolayer Eu^{3+}:Lu_2SiO_5/Glymo, and (**C**) mapping of the Eu^{3+}:Lu_2SiO_5 film.

As expected, a dense film with a homogenous distribution of nanometric particles and crack-free Lu_2SiO_5:Eu^{3+} layer was formed without Glymo as can be seen in Figure 7A.

The sample with Glymo shown in Figure 7B suggests that the larger amount of ethyl groups present in the Glymo precursor produced TEOS chains, which disrupt the stability of the Lu_2SiO_5 film's surface, thus modifying the evaporation of the organic compounds.

A fluffy and porous morphology resulted from the modified surface with Glymo because of the controlled heat treatment at a different temperature which eliminated the organic component of the surfactant on the Lu_2SiO_5:Eu^{3+}/Glymo coatings. Reaffirming the results of X-ray diffraction by means of EDS mapping analyses, Figure 7c shows that the homogeneity distribution of the Eu-doped ion is equally distributed on the surface of the lutetium mono-silicate films.

The surface roughness of Eu^{3+}:Lu_2SiO_5 and Eu^{3+}:Lu_2SiO_5/Glymo films are presented in Figure 8A,B respectively. It should be noticed that the film without surfactant is crack free, homogeneous, and mainly consists of closely packed fine particles, and the surface is well crystallized and very smooth with an RMS roughness of 4.28 nm.

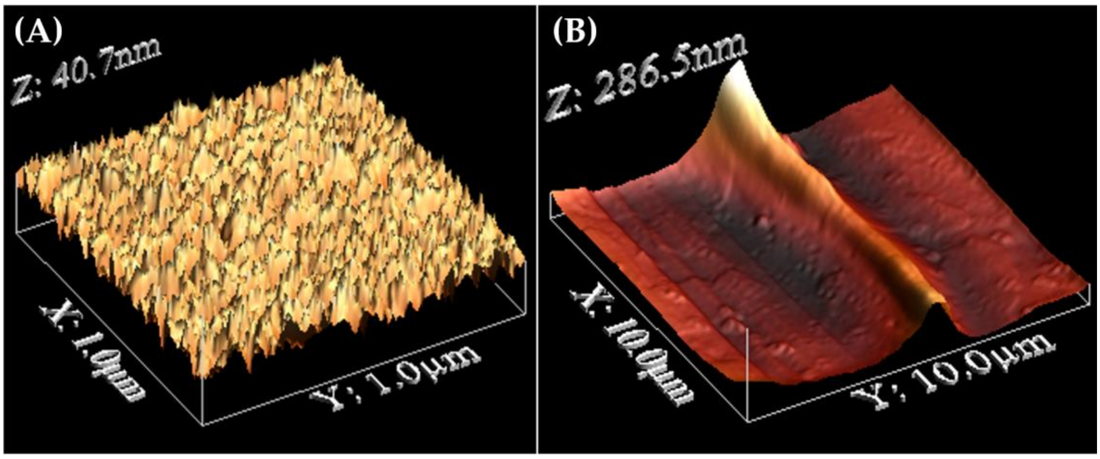

Figure 8. AFM images of (**A**) Eu^{3+}:Lu_2SiO_5 and (**B**) Eu^{3+}:Lu_2SiO_5/Glymo films.

However, the film containing Glymo as a surfactant exhibited the shape of the hills and valleys with a roughness of 17.4 nm, and particles were not observed due to the surface having a plasticized, coated shape. As previously described in XRD results, the incorporation of Glymo benefits the formation of the Lu–Glymo–Si complex, where the growth of the 3D network took place inducing huge separations between lutetium silicate particles as shown in Figure 8B.

The absorption spectra of LS2 and LSG2 films are shown in Figure 9A. An Eu^{3+}—O charge transfer band (CT) was identified at 258 nm in both systems [30,32]. For the LS2 system, the electronic transitions between $^5D_4 \leftarrow {}^7F_0$, $^5G_2 \leftarrow {}^7F_0$, and $^5L_6 \leftarrow {}^7F_0$ levels are identified at 361 nm, 380 nm, and 393 nm, respectively [33]. The incorporation of Glymo into the system benefits the J-mixing effect, which can be identified in the absorption spectra of the LSG2 system where the absorption band at 414 nm is higher than the Eu^{3+}—O CT band. This band corresponds to the $^5D_3 \leftarrow {}^7F_0$ transition; however, this transition is weak due to being an electric dipole transition and the absence of inversion symmetry at the Eu^{3+} sites is due to the incorporation of the surfactant [9]. According to the Judd–Ofelt theory, the $^5D_3 \leftarrow {}^7F_0$ transition can be made more intense by the J-mixing effect [34,35]. Under UV irradiation (λ_{exc} = 258 nm for films), the Lu_2SiO_5:Eu^{3+} film (LS2) exhibits strong red emission, unlike the Lu_2SiO_5:Eu^{3+}/Glymo system film (LSG2) where it is evident that the incorporation of Glymo as a surfactant decreases the luminescence intensity due to the inefficient energy transfer as shown on the emission spectra of the systems in Figure 9B. Moreover, it can be associated with the presence of different phases; this effect is better observed in the XRD pattern of the p-LSG2 powder (Figure 4). The emission bands observed in both systems correspond to the Eu^{3+} 4f–4f transitions [30].

On the other hand, the intensity ratio R of the $^5D_0 \rightarrow {}^7F_2$ to $^5D_0 \rightarrow {}^7F_1$ transitions can provide some information on the local crystal field environment around the Eu^{3+} ion located in the host lattice since it is well known that the $^5D_0 \rightarrow {}^7F_2$ red and $^5D_0 \rightarrow {}^7F_1$ orange-red emissions are electric dipole and magnetic dipole transitions, respectively, with the first one being a hypersensitive transition and, therefore, very sensitive to the site symmetry, and the second one being insensitive to the symmetry of the crystal environment [36]. The calculated R values diminish from 3.66 for the Glymo-free sample to 1.1 for the Glymo-modified sample. Therefore, the asymmetry of the Eu^{3+} environment is higher for the Glymo-free sample, indicating that the Glymo presence tends to promote the Eu^{3+} cation to localize in a centrosymmetric site or at a high symmetry site. This effect can be explained by the fact, as observed in XRD, that the Glymo presence tends to retard the condensation reactions on the Lu_2SiO_5 system.

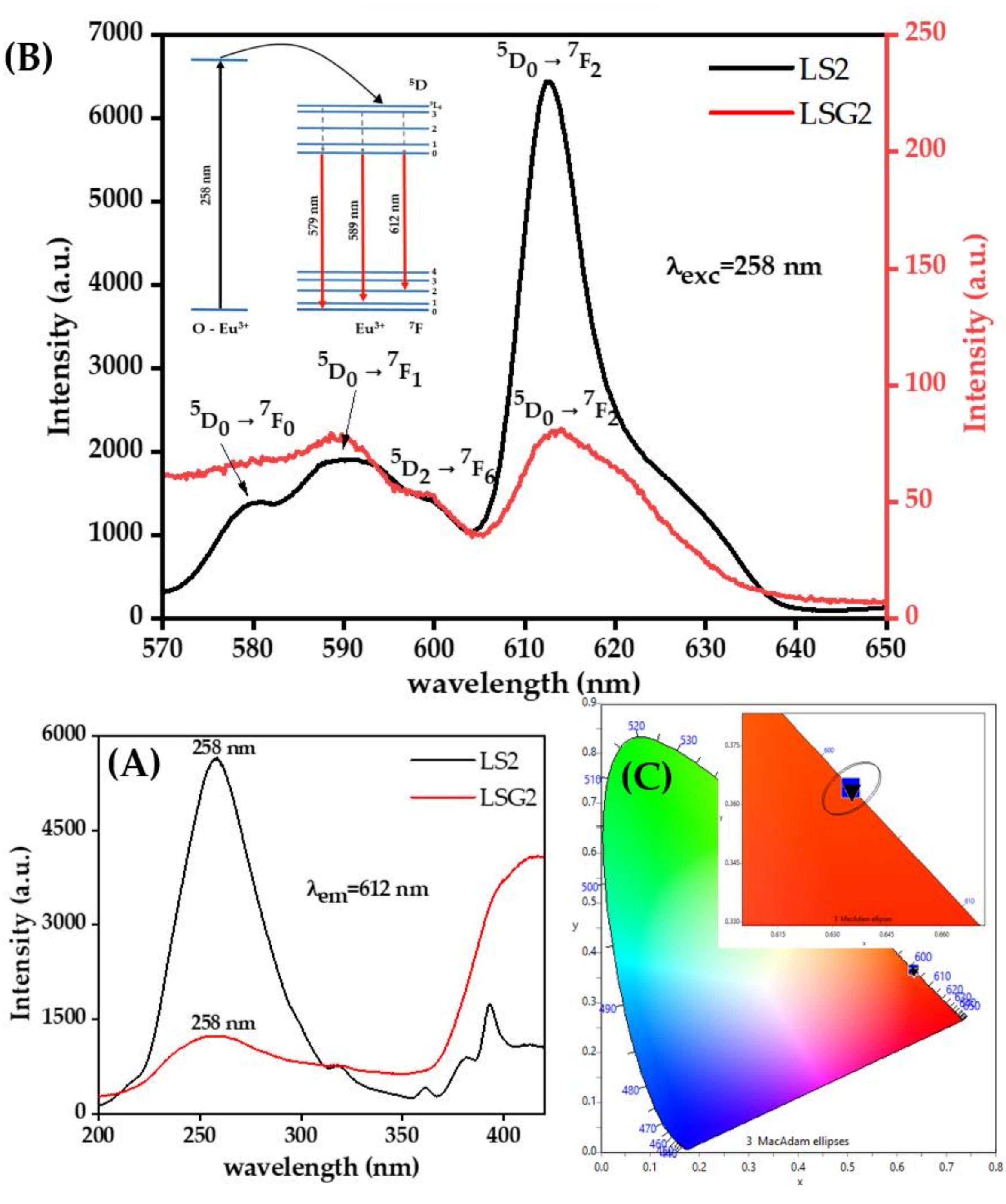

Figure 9. (**A**) PL excitation spectra, (**B**) PL emission spectra and energy transfer mechanism, and (**C**) CIE diagram of Eu^{3+}:Lu_2SiO_5 (LS2) and Eu^{3+}:Lu_2SiO_5/Glymo (LSG2) systems.

The chromaticity diagram according to the International Commission on Illumination (CIE 1931) is shown in Figure 9c for Eu^{3+}-doped and Eu^{3+}/Glymo-doped lutetium monosilicate films (LS2 and LSG2 samples).

The chromaticity diagram provides a visual understanding of the properties of the colors [37]. For all systems, the color coordinates (x, y) are in the red region of the diagram, very close to the edge of the diagram, which is known as the spectral locus, and in the CIE diagram it represents pure monochromatic light, that is, the closer the color coordinates are to the spectral locus, the more color is in the spectrum. The color coordinates for the LS2 system are x = 0.6531, y = 0.3643 and for the LSG2 system the coordinates are x = 0.6355, y = 0.3640, which are in the reddish region represented in the CIE diagram.

Finally, the luminescence decay of the Eu^{3+} was monitored for the Eu^{3+}:Lu_2SiO_5 film (LS2) and the Eu^{3+}:Lu_2SiO_5/Glymo system film (LSG2) by exciting at 258 nm and collecting the emission of the $^5D_4 \rightarrow ^7F_5$ transition at 612 nm, as shown in Figure 10a,b, respectively. Both can be fitted by a mono-exponential function in the region from 0 to 15 ms according to the following equation:

$$I(t) = I_0 e^{-t/\tau} \quad (2)$$

where $I(t)$ and I_0 are the luminescence intensities at time t and τ = 0, respectively, while τ is the luminescence decay time (ms). This study shows the lifetime increases from the Glymo-free sample (2.1819ms ± 0.00307, R^2 = 0.99908) to the Glymo-modified sample (3.48548 ± 0.00447, R^2 = 0.99936). Longer emission lifetimes indicate a lower probability of non-radiative energy transfer; therefore, it can be expected that the Glymo presence tends to minimize the content of remnant hydroxyl groups and promotes a better homogeneity of the Eu distribution on Lu_2SiO_5.

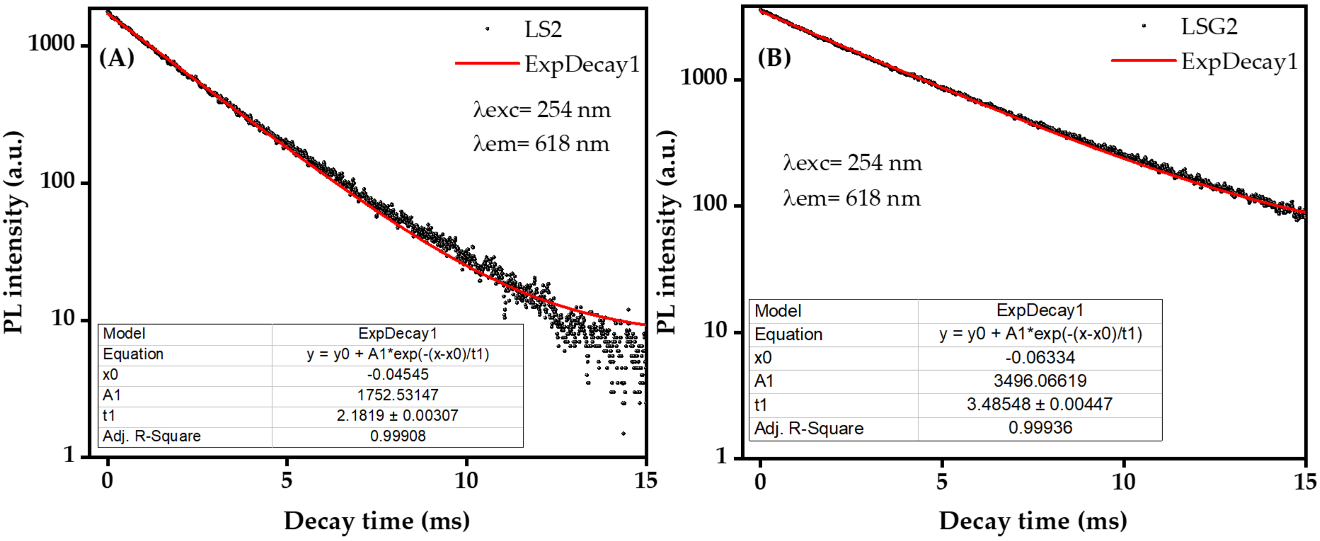

Figure 10. Decay curves of (**A**) Eu^{3+}:Lu_2SiO_5 (LS2) and (**B**) Eu^{3+}:Lu_2SiO_5/Glymo (LSG2) systems.

4. Conclusions

Lu_2SiO_5, Eu^{3+}:Lu_2SiO_5, and Eu^{3+}:Lu_2SiO_5/Glymo films and powders were prepared successfully by the sol–gel method in combination with the dip-coating technique. The Lu_2SiO_5 systems crystallized first in $P2_1/c$ (A-type) followed by an incomplete phase transition to the C2/c phase (B-type) at 1100 °C. The incorporation of the Eu^{3+} ion does not affect the crystalline phase of the system, unlike the incorporation of Glymo as a surfactant, which influences the crystalline phase of the system according to the XRD results, obtaining a mixture of the Lu_2SiO_5 and $Lu_2Si_2O_7$ systems. A characteristic red luminescence was obtained for the Lu_2SiO_5:Eu^{3+} and Lu_2SiO_5:Eu^{3+}/Glymo systems. Nevertheless, the Lu_2SiO_5:Eu^{3+} (LS2) sample exhibited a major luminescent emission line in λ_{em} = 612 nm.

Author Contributions: Conceptualization, M.G.-H. and Á.d.J.M.-R.; methodology, A.D.C.-M.; validation, M.G.-H., Á.d.J.M.-R. and A.L.-M.; formal analysis, J.H.L.-D.; investigation, A.D.C.-M. and J.A.Á.-C.; resources, M.O.-A. and J.A.Á.-C.; writing—original draft preparation, M.G.-H. and A.D.C.-M.; writing—review and editing, M.G.-H. and Á.d.J.M.-R.; visualization, J.H.L.-D.; supervision, M.G.-H. and A.L.-M. All authors have read and agreed to the published version of the manuscript.

Funding: This research received no external funding.

Institutional Review Board Statement: Not applicable.

Informed Consent Statement: Not applicable.

Data Availability Statement: Not applicable.

Acknowledgments: The authors acknowledge IPN and SIP-IPN for 20232204, 20231168, 20231939, and 20232646 projects for supporting this work. The experimental support of CNMN-IPN in the execution of the presented work is also acknowledged.

Conflicts of Interest: The authors declare no conflict of interest.

References

1. Singh, J.; Sahu, K.; Singh, R.; Som, T.; Kotnala, R.K.; Mohapatra, S. Thermal annealing induced strong photoluminescence enhancement in Ag-TiO2 plasmonic nanocomposite thin films. *J. Alloys Compd.* **2019**, *786*, 750–757. [CrossRef]
2. Meng, Q.; Lin, J.; Fu, L.; Zhang, H.; Wang, S.; Zhou, Y. Sol-gel deposition of calcium silicate red-emitting luminescent films doped with Eu3+. *J. Mater Chem.* **2001**, *11*, 3382–3386. [CrossRef]
3. Shen, S.Q.; Xu, Z.B.; Ma, Q.; Xie, J.J.; Shi, Y.; Xu, J.Y.; Ai, F. Pechini sol-gel fabrication and luminescent properties of Lu2SiO5:Ln3+ (Ln = Tb,Ce) thin films. *Appl. Mech. Mater.* **2011**, *84–85*, 631–634. [CrossRef]
4. Melcher, C.; Schweitzer, J. Cerium-doped Lutetium Oxyorthosilicate: A Fast, Efficient New Scintillator. *IEEE Trans. Nucl. Sci.* **1992**, *39*, 502–505. [CrossRef]
5. Kitaura, M.; Tanaka, S.; Itoh, M. Optical properties and electronic structure of Lu2SiO5 crystals doped with cerium ions: Thermally-activated energy transfer from host to activator. *J. Lumin.* **2015**, *158*, 226–230. [CrossRef]
6. Chewpraditkul, W.; Moszynski, M. Scintillation Properties of Lu3Al5O12, Lu2SiO5 and LaBr3 Crystals Activated with Cerium. *Phys. Procedia* **2011**, *22*, 218–226. [CrossRef]
7. Dominiak-Dzik, G.; Ryba-Romanowski, W.; Lisiecki, R.; Solarz, P.; Berkowski, M. Dy-doped Lu2SiO5 single crystal: Spectroscopic characteristics and luminescence dynamics. *Appl. Phys. B* **2010**, *99*, 285–297. [CrossRef]
8. Mansuy, C.; Tomasella, E.; Mahiou, R.; Grimblot, J.; Nedelec, J.-M. Surface characterization of sol-gel derived scintillating rare-earth doped Lu2SiO5 thin films. *J. Physics Conf. Ser.* **2008**, *100*, 012037. [CrossRef]
9. Cooke, D.; Muenchausen, R.; McClellan, K.; Bennett, B. Spectral emission of rare-earth doped Lu2SiO5 single crystals. *Opt. Mater.* **2005**, *27*, 1781–1786. [CrossRef]
10. Mansuy, C.; Leroux, F.; Mahiou, R.; Nedelec, J.M. Preferential site substitution in sol-gel derived Eu3+ doped Lu2SiO5: A combined study by X-ray absorption and luminescence spectroscopies. *J. Mater. Chem.* **2005**, *15*, 4129–4135. [CrossRef]
11. Yun, P.; Shi, Y.; Zhou, D.; Xie, J. Hydrothermal synthesis of Ce:Lu2SiO5 scintillator powders. *J. Rare Earths* **2009**, *27*, 801–805. [CrossRef]
12. Lee, J.-K.; Muenchausen, R.E.; Jia, Q.X.; Nastasi, M.; Valdez, J.A.; Bennett, B.L.; Cooke, D.W.; Lee, S.Y. Structure and optical properties of Lu2SiO5:Ce phosphor thin films. *Appl. Phys. Lett.* **2006**, *89*, 101905. [CrossRef]
13. Felsche, J. *The Crystal Chemistry of the Rare-Earth Silicates*; Springer: Berlin/Heidelberg, Germany, 1973; pp. 99–197.
14. Lu, Q.; Liu, Q.; Wei, Q.; Liu, G.; Zhuang, J. Preparation and characterization of Lu2SiO5:Ce3+ luminescent ceramic fibers via electrospinning. *Ceram. Int.* **2013**, *39*, 8159–8164. [CrossRef]
15. Fan, L.; Lin, D.; Zhang, X.; Shi, Y.; Zhang, J.; Xie, J.; Lei, F.; Zhang, L. Local structures of Lu atoms in a core-shell approach for synthesis of Lu2SiO5 phase. *Chem. Phys. Lett.* **2016**, *644*, 41–44. [CrossRef]
16. Jota, M.L.C.; Hernández, M.G.; Murillo, A.G.; Romo, F.D.J.C.; Becerril, E.R.; Ramírez, A.D.J.M.; Enriquez, H.D.; De La Rosa Cruz, E. Synthesis of Lu2O3:Eu3+ Luminescent Ceramic Powder Embedded in SiO2 Matrix. *Mater. Trans.* **2014**, *55*, 1867–1871. [CrossRef]
17. Jota, M.C.; Murillo, A.G.; Romo, F.C.; Hernández, M.G.; Ramírez, A.D.J.M.; Velumani, S.; Cruz, E.D.L.R.; Kassiba, A. Lu2O3:Eu3+ glass ceramic films: Synthesis, structural and spectroscopic studies. *Mater. Res. Bull.* **2014**, *51*, 418–425. [CrossRef]
18. Shin, D.-Y.; Cao, G.; Kim, K.-N. Prepration and photoluminescence properties of Ce doped lutetium silicate nanopowders by sol-gel method. *Curr. Appl. Phys.* **2011**, *11*, S309–S312. [CrossRef]
19. Brinker, C.J. Hydrolysis and condensation of silicates: Effects on structure. *J. Non-Crystalline Solids* **1988**, *100*, 31–50. [CrossRef]
20. Bahtat, M.; Mugnier, J.; Lou, L.; Bovier, C.; Serughetti, J.; Genet, M. La Spectroscopie Raman Tres Basse Frequence Utilisee Pour La Caracterisation Structurale De Guides D 'Ondes Plans. *J. Opt.* **1992**, *23*, 215–222. [CrossRef]
21. Bishnoi, A.; Kumar, S.; Joshi, N. *Wide-Angle X-ray Diffraction (WXRD). Microscopy Methods in Nanomaterials Characterization*; Elsevier Inc.: Amsterdam, The Netherlands, 2017.
22. Khamis, F.; Arafah, D.E. Thermoluminescence Characteristics of Natural Quartz and Synthesized Silica Glass Prepared by Sol-Gel Technique. *Asian J. Phys. Chem. Sci.* **2017**, *3*, 1–16. [CrossRef]
23. Arunkumar, P.; Ramaseshan, R.; Dash, S.; Babu, K.S. Tunable transport property of oxygen ion in metal oxide thin film: Impact of electrolyte orientation on conductivity. *Sci. Rep.* **2017**, *7*, 1–18. [CrossRef]
24. Liu, H.; Wan, D.; Ishaq, A.; Chen, L.; Guo, B.; Shi, S.; Luo, H.; Gao, Y. Sputtering Deposition of Sandwich-Structured V2O5/Metal (V, W)/V2O5 Multilayers for the Preparation of High-Performance Thermally Sensitive VO2 Thin Films with Selectivity of VO2 (B) and VO2 (M) Polymorph. *ACS Appl. Mater. Interfaces* **2016**, *8*, 7884–7890. [CrossRef]
25. Xu, Y.; Li, J. Preparation and molten salt corrosion research of composite environmental barrier coatings of Lu2Si2O7 and Lu2SiO2. *Mater. Res. Innov.* **2014**, *18*, S4958–S4962. [CrossRef]

26. Xie, J.; Shi, Y.; Fan, L.; Xu, Z. Microstructure and luminescent properties of Ce:Lu2SiO5 ceramic scintillator by spark plasma sintering. *Opt. Mater.* **2013**, *35*, 744–747. [CrossRef]
27. Wang, Y.; He, Q.; Chu, B. Synthesis and characterization of Ce-doped Lu2SiO5 powders by the solid-state reaction with Li2SO4 flux. *J. Alloys Compd.* **2009**, *479*, 704–706. [CrossRef]
28. Fan, L.; Shi, Y.; Xu, J.; Xie, J.; Lei, F. Consolidation of translucent Ce3+-doped Lu2SiO5 scintillation ceramics by pressureless sintering. *J. Mater. Res.* **2014**, *29*, 2252–2259. [CrossRef]
29. Liu, X.; Fan, Y.; Chen, S.; Gu, M.; Ni, C.; Liu, B.; Huang, S. Luminescence properties of Li-codoped Lu2SiO5:Ce thin-film phosphors prepared by sol-gel processing. *Mater. Res. Bull.* **2013**, *48*, 2370–2374. [CrossRef]
30. Mansuy, C.; Dujardin, C.; Mahiou, R.; Nedelec, J.M. Characterization and scintillation properties of sol-gel derived Lu2SiO5:Ln3+ (Ln = Ce, Eu and Tb) powders. *Opt. Mater.* **2009**, *31*, 1334–1336. [CrossRef]
31. Zhang, X.; Xie, J.; Chen, X.; Fan, L.; Lin, D.; Wang, Y.; Shi, Y. Fabrication and luminescence properties of polycrystalline Pr3+-doped Lu2SiO5 thin films by sol-gel method. *J. Alloys Compd.* **2016**, *656*, 735–739. [CrossRef]
32. Hoefdraad, H.E. The charge-transfer absorption band of Eu3+ in oxides. *J. Solid. State Chem.* **1975**, *14*, 217.
33. Rajagukguk, J.; Kaewkhao, J.; Djamal, M.; Hidayat, R.; Suprijadi; Ruangtaweep, Y. Structural and optical characteristics of Eu3+ ions in sodium-lead-zinc-lithium-borate glass system. *J. Mol. Struct.* **2016**, *1121*, 180–187. [CrossRef]
34. Shangda, X.; Yimin, C. Effect of J-mixing on the intensities of f-f transitions of the rare earth ions. *J. Lumin.* **1984**, *32*, 204–206. [CrossRef]
35. Souza, A.; Santos, M. The J-mixing effect in Ln3+ ions crystal field levels. *Chem. Phys. Lett.* **2012**, *521*, 138–141. [CrossRef]
36. Sakthivel, T.; Sun, L.; Devakumar, B.; Li, B.; Huang, X. Novel high-efficiency Eu3+-activated Na2Gd2B2O7 red-emitting phosphors with high color purity. *RSC Adv.* **2018**, *8*, 32948–32955. [CrossRef]
37. Nixon, M.S.; Aguado, A.S. *Appendix 4: Color Images. Feature Extraction & Image Processing for Computer Vision*; Elsevier Ltd.: Amsterdam, The Netherlands, 2012.